

**Snow cover reconstruction methodology**

A. Gafurov et al.

# Snow cover reconstruction methodology based on historic in situ observations and recent remote sensing data

**A. Gafurov<sup>1</sup>, S. Vorogushyn<sup>1</sup>, A. Merkushkin<sup>2</sup>, D. Duethmann<sup>1</sup>, D. Farinotti<sup>1</sup>, and B. Merz<sup>1</sup>**

<sup>1</sup>GFZ German Research Centre for Geosciences, Sect. 5.4: Hydrology, Potsdam, Germany

<sup>2</sup>Uzbek Hydrometeorological Service (Uzhydromet), Tashkent, Uzbekistan

Received: 29 July 2014 – Accepted: 31 July 2014 – Published: 1 September 2014

Correspondence to: A. Gafurov (gafurov@gfz-potsdam.de)

Published by Copernicus Publications on behalf of the European Geosciences Union.

Title Page

Abstract

Introduction

Conclusions

References

Tables

Figures



Back

Close

Full Screen / Esc

Printer-friendly Version

Interactive Discussion



## Abstract

Spatially distributed snow cover extent can be derived from remote sensing data with good accuracy. However, such data are available for recent decades only, after satellite missions with proper snow detection capabilities were launched. Yet, longer time series of snow cover area (SCA) are usually required e.g. for hydrological model calibration or water availability assessment in the past. We present a methodology to reconstruct historical snow coverage using recently available remote sensing data and long-term point observations of snow depth from existing meteorological stations. The methodology is mainly based on correlations between station records and spatial snow cover patterns. Additionally, topography and temporal persistence of snow patterns are taken into account. The methodology was applied to the Zerafshan River basin in Central Asia – a very data-sparse region. Reconstructed snow cover was cross-validated against independent remote sensing data and shows an accuracy of about 85%. The methodology can be used to overcome the data gap for earlier decades when the availability of remote sensing snow cover data was strongly limited.

## 1 Introduction

Water resources from remote mountain catchments play a crucial role for the development of regions in or in the vicinity of mountain ranges (Pellicciotti et al., 2011). Seasonal snow is an important water resource in many of Earth's semiarid regions (Durand et al., 2008). Particularly, in Central Asia, seasonal snowmelt decisively contributes to the total runoff volume (Ososkova et al., 2000; Unger-Shayesteh et al., 2013).

Information on snow cover and snow depth and ideally on snow water equivalent in Central Asian catchments is crucial for seasonal forecasts of water availability and for calibration and validation of hydrological models. However, the available sparse station-based data are insufficient to represent the snow cover variability over the large and remote mountain areas (Erickson et al., 2005). The development of remote sensing

TCD

8, 4645–4680, 2014

## Snow cover reconstruction methodology

A. Gafurov et al.

Title Page

Abstract

Introduction

Conclusions

References

Tables

Figures



Back

Close

Full Screen / Esc

Printer-friendly Version

Interactive Discussion



## Snow cover reconstruction methodology

A. Gafurov et al.

Title Page

Abstract

Introduction

Conclusions

References

Tables

Figures



Back

Close

Full Screen / Esc

Printer-friendly Version

Interactive Discussion



techniques during recent decades allows to derive snow cover (Liu et al., 2012), but reliable remote sensing data with adequate spatial and temporal resolution such as MODIS (Moderate Resolution Imaging Spectroradiometer) are available for recent decades only. The derivation of snow cover from Landsat and Advanced Very High Resolution Radiometer (AVHRR) data which are available for longer periods (Landsat launch 1972; AVHRR launch 1978) is strongly limited by the presence of clouds and atmospheric pollutants. Although recently the reconstruction of snow cover time series from AVHRR data for Central Asia has been reported by Zhou et al. (2013). However, they are also limited in time starting in 1986 at earliest.

Several studies used remotely sensed snow cover either as input to hydrological models (Tekeli et al., 2005; Immerzeel et al., 2008; Li et al., 2008; Wang et al., 2010) or for calibration and validation purposes (Parajka and Blöschl, 2008a; Corbari et al., 2009; Liu et al., 2012; Duethmann et al., 2014). Particularly, for hydrological model calibration, spatially distributed snow cover data offer high information content required to constrain model parameters (Finger et al., 2011; Duethmann et al., 2014).

In Central Asia, continuous hydro-meteorological records are widely available from 1960s and earlier until the collapse of the Soviet Union in 1991. In contrast, continuous remote sensing snow cover data from MODIS are readily available after 2000, when station data are very scarce. We present a methodology which enables reconstructing historical snow cover pattern using long-term, point-based observations from existing meteorological stations and recent remotely sensed snow cover data. By merging high-resolution spatial satellite data with long-term station data, snow cover patterns can be reconstructed for several decades into the past.

Only a limited number of studies on snow cover reconstruction have been conducted in the past that use long term station observations and recent remote sensing data (Robinson, 1991; Brown, 1999; Frei et al., 1999). These studies are however conducted at the continental scale under conditions of dense station network availability and neglecting the effect of topography. Robinson (1991) and Frei et al. (1999) conducted reconstruction of snow cover based on regression analysis between snow

## Snow cover reconstruction methodology

A. Gafurov et al.

Title Page

Abstract

Introduction

Conclusions

References

Tables

Figures



Back

Close

Full Screen / Esc

Printer-friendly Version

Interactive Discussion



characteristics and snow cover area derived from AVHRR satellite observations. As snow characteristics both studies used snow cover duration derived from interpolated station records. Another study by Brown (1999) conducted reconstruction of snow cover for “pre-satellite era” interpolating snow depth data from station network. For grid cells of nearly 200 km, the interpolation of snow cover was done using different thresholds for snow depth and compared against AVHRR snow cover during “satellite era”. The calibration showed 2 cm to be most appropriate snow depth for accurate snow cover reconstruction based on station data. These studies can be helpful in assessing climate related variations of snow cover but are hardly transferable to smaller catchment scale with moderate resolution and limited station data availability.

Different to those studies mentioned above, we present a methodology for snow cover reconstruction (1) with moderate spatial resolution (500 m), (2) suitable for catchment scale hydrological studies, (3) accounting topography and (4) delivering spatially distributed snow cover maps. The methodology takes advantage of the strong control of topography on the spatial snow cover distribution. Hence, measurements from snow observation stations at different elevations can be interpreted as representative sites to predict snow cover patterns. The methodology consists of five successive steps which make use of topographic information and correlations between station records and spatial snow cover patterns. In order to test the presented methodology, snow cover reconstruction was conducted for four days (Table 1) for which independent Landsat data were available.

## 2 Study area

The methodology for snow cover reconstruction was developed and tested for the area containing the Upper Zerafshan River basin, Central Asia (Fig. 1).

The Upper Zerafshan River basin is located in the Gissaro-Alai Mountain Range. Elevation ranges from 658 to 5402 m a.s.l. and basin area is about 12 000 km<sup>2</sup>. The Zerafshan River basin is currently an endorheic basin in the inner Central Asia that

## Snow cover reconstruction methodology

A. Gafurov et al.

Title Page

Abstract

Introduction

Conclusions

References

Tables

Figures

⏪

⏩

◀

▶

Back

Close

Full Screen / Esc

Printer-friendly Version

Interactive Discussion



no longer contributes to the Amudarya River. It originates in Tadjikistan and flows towards Uzbekistan, where its water is used for agricultural production in the oases of Samarkand and Bukhara. The flow regime is strongly dominated by snow and glacier melt, as can be inferred from the temperature, precipitation and flow regimes in Fig. 2.

5 The highest precipitation is brought by westerly flows during winter and spring, with a clear minimum during summer and early autumn (Aizen et al., 1995). The highest runoff, however, occurs during summer months and is driven by snow and glacier melt.

### 3 Data

10 We used (1) daily in situ snow depth data, (2) daily MODIS snow cover data, (3) a digital elevation model (DEM), and (4) Landsat data. The first three datasets were used for snow cover reconstruction whereas Landsat data was used as an independent dataset to validate the results.

#### 3.1 In situ snow depth data

15 Daily snow depth data in the period from 1964 to 2012 were available for seven climate stations located at different elevations (Fig. 1, Table 1). The data were provided by Uzbek Hydrometeorological Service (Uzhydromet).

#### 3.2 MODIS snow cover data

20 MODIS daily snow cover data from the Terra satellite with 500 m spatial resolution (MOD10A, version V005) were employed for the time period of 2000 to 2012. We used MODIS Terra snow cover data due to its longer time series compared to the Aqua satellite, which delivered snow cover data only after 2002. The MODIS snow cover product is based on the Normalized Difference Snow Index (NDSI) algorithm (Hall et al., 2002a). Its accuracy was tested in different parts of the world showing good agreement with in situ data (Klein et al., 2003; Tekeli et al., 2005; Parajka et al., 2006; Ault et al., 2006;

## Snow cover reconstruction methodology

A. Gafurov et al.

Title Page

Abstract

Introduction

Conclusions

References

Tables

Figures



Back

Close

Full Screen / Esc

Printer-friendly Version

Interactive Discussion



Wang et al., 2008; Liang et al., 2008; Huang et al., 2011; Gafurov et al., 2013; Parajka et al., 2012). The main drawback of MODIS snow cover data is the limitation due to cloud cover. There have been several studies on filtering methods for reducing cloud cover or even removing it completely (e.g., Parajka and Blöschl, 2008a, b; Gafurov and Bárdossy, 2009; Tong et al., 2009; Hall et al., 2010; Lòpez-Burgos et al., 2013). We used original MODIS snow cover data to exclude any uncertainty that may be introduced by cloud filtering. The data were obtained from National Aeronautics and Space Administration (NASA)'s Earth Observing System Data and Information System (EOS-DIS) Reverb platform. MODIS data are distributed as tiles with the size of 10° by 10°, which makes up a total of 36 horizontal (h) and 18 vertical (v) tiles covering the entire globe. In this study, the tile h23v05 was used which covers the study area completely.

### 3.3 Digital elevation model

The void-filled DEM with 90 m spatial resolution from NASA Shuttle Radar Topography Mission (SRTM) was used. SRTM DEM data was obtained from the CGIAR CSI (Consultative Group on International Agricultural Research, Consortium for Spatial Information) Database ([www.cgiar-csi.org/data](http://www.cgiar-csi.org/data)). To have the same resolution as the MODIS data (500 m), the 90 m SRTM DEM was aggregated to 500 m.

### 3.4 Landsat data

Optical remote sensing data from the Landsat Thematic Mapper (TM) sensor were used to validate the reconstructed snow cover maps. The Landsat data have a spatial resolution of 30 m and a temporal resolution of 16 days. Landsat data from four nearly clear-sky days in the snow season (10 April 1998, 20 November 1998, 20 April 1999 and 15 November 1999) were used for validation purposes. Snow cover maps for the Landsat footprint (see Fig. 1) were prepared using the NDSI methodology. For a detailed description of the algorithm used for deriving snow cover maps from Landsat



3. Pixel to pixel MR fields
4. Usage of elevation information
5. Station to pixel MR fields for  $MR < 1$

#### 4.1 Station to pixel matching ratio

5 Let us define the “matching ratio” (MR) of a pixel at  $x, y$  and station  $n$  as:

$$MR_{(x,y),(n)}^s = \frac{\sum (1 - ABS(S_{x,y,t} - S_{n,t}))}{N_{x,y}} \quad \forall S_{n,t} = 1 \quad (1)$$

$$MR_{(x,y),(n)}^l = \frac{\sum (1 - ABS(S_{x,y,t} - S_{n,t}))}{N_{x,y}} \quad \forall S_{n,t} = 0 \quad (2)$$

10 where  $MR_{(x,y),(n)}^s$  and  $MR_{(x,y),(n)}^l$  are matching ratios between a pixel with coordinates  $x, y$  and station  $n$  for snow and snow free (i.e. land) conditions, respectively.  $S_{x,y,t}$  and  $S_{n,t}$  are binary variables indicating the presence ( $S = 1$ ) or absence ( $S = 0$ ) of snow for day  $t$ , respectively.  $N_{x,y}$  is the number of observations simultaneously available at pixel  $x, y$  (excluding cloud covered days) and station  $n$  over the 12 years (2000–2012), for which station  $n$  showed snow ( $S = 1$ ) or snow free ( $S = 0$ ) conditions, respectively. The value of  $MR_{(x,y),(n)}^s$  ( $MR_{(x,y),(n)}^l$ ) varies from 0 to 1, and gives the proportion of matches between the snow cover (snow free) observation derived from MODIS, and the snow cover (snow free) observed at a given station.  $MR_{(x,y),(n)}^s = 1$  ( $MR_{(x,y),(n)}^l = 1$ ) indicates that a pixel at  $x, y$  was always observed as snow covered (snow free) by MODIS when station  $n$  measured snow depth  $> 0$  ( $= 0$ ), whilst  $MR_{(x,y),(n)}^s = 0$  ( $MR_{(x,y),(n)}^l = 0$ ) indicates an opposite relationship, i.e. that the MODIS product at  $x, y$  showed snow free (snow cover) when station  $n$  always had snow depth  $> 0$  ( $= 0$ ).

In meteorology and hydrology, correlations between two or more stations are commonly examined to fill data gaps. Here, MRs were computed between snow monitoring

stations and each MODIS pixel in the study area (total of 169 776 pixels) over 12 years of available MODIS observations. Hence, the daily snow cover maps from MODIS are treated as snow observation for each 500 m grid cell, giving rise to a very dense “observation network”. An example for a MR map for snow and land conditions for Chimgan station is given in Fig. 4. In total, 14 maps were derived (two maps for every of the 7 stations: one for  $MR_{(x,y),(n)}^s$  and one for  $MR_{(x,y),(n)}^l$ ).

The number of pixels with  $MR_{(x,y),(n)}^s = 1$  ( $MR_{(x,y),(n)}^l = 1$ ) varies from station to station. The higher the number of pixels with  $MR_{(x,y),(n)}^s = 1$ , the higher is the predictive power of the station for snow classification. Similarly, the higher the number of pixels with  $MR_{(x,y),(n)}^l = 1$ , the higher is the predictive power of the station to predict snow-free conditions. In order to quantify the predictive power of each station, we introduce two terms: Snow Predictability Index (SPI) and Land Predictability Index (LPI). These terms give the fractions of the reconstruction domain with  $MR = 1$  for a given station for snow and land conditions, respectively:

$$SPI_n = \frac{\sum (MR_{(x,y),(n)}^s = 1)}{N} \cdot 100 \quad [\%] \quad (3)$$

$$LPI_n = \frac{\sum (MR_{(x,y),(n)}^l = 1)}{N} \cdot 100 \quad [\%] \quad (4)$$

where  $SPI_n$  and  $LPI_n$  are Snow Predictability Index and Land Predictability Index of station  $n$ .  $N$  is the total number of pixels (169 776) in the entire study area. Pixels with  $MR_{(x,y),(n)}^s = 1$  in Fig. 4 (top) add up to 10.2% which is the SPI value of Chimgan station for the entire domain. This means that when Chimgan station shows a snow depth above zero, 10.2% of the study area can be classified as snow covered as well. Pixels with  $MR_{(x,y),(n)}^l = 1$  in Fig. 4 (bottom) add up to 9.0%, i.e. when Chimgan station shows snow-free conditions, 9.0% of the study area can be assigned as snow free.

**Snow cover reconstruction methodology**

A. Gafurov et al.

Title Page	
Abstract	Introduction
Conclusions	References
Tables	Figures
◀	▶
◀	▶
Back	Close
Full Screen / Esc	
Printer-friendly Version	
Interactive Discussion	



## Snow cover reconstruction methodology

A. Gafurov et al.

Title Page

Abstract

Introduction

Conclusions

References

Tables

Figures

◀

▶

◀

▶

Back

Close

Full Screen / Esc

Printer-friendly Version

Interactive Discussion



Figure 4 shows that  $MR_{(x,y),(n)}^S = 1$  occurs mainly at high elevations (cf. Fig. 1), whilst  $MR_{(x,y),(n)}^I = 1$  occurs mainly at low elevations. Pixels with an elevation far higher than the elevation of Chimgan station tend to be snow covered if Chimgan station records positive snow depth, whilst pixels with an elevation far below the elevation of Chimgan station tend to be snow free if Chimgan station records snow depth of zero. Table 1 shows the SPI and LPI values for each station. The stations Kul' and Minchukur near the Zerafshan basin (see Fig. 1) have the highest SPI values (23.2 and 22.6, respectively). Other stations, located further away from the catchment, have smaller SPI values. Noticeably, Oigaing station located farthest away from the Zerafshan basin has the highest LPI value (12.3 %). This can be explained with the high elevation of the station. When the station indicates snow free conditions, pixels with significantly lower elevation are likely to be snow-free as well. Assuming that the dependencies remain stable in time, the computed MRs between station and MODIS data can be used to classify individual pixels for any arbitrary day prior to the availability of MODIS data (before 2000) for which station records are available:

$$S_{(x,y,t)} = 1 \quad \text{if} \quad \left( MR_{(x,y,n)}^S = 1 \quad \text{and} \quad S_{(n,t)} = 1 \right) \quad (5)$$

$$S_{(x,y,t)} = 0 \quad \text{if} \quad \left( MR_{(x,y,n)}^I = 1 \quad \text{and} \quad S_{(n,t)} = 0 \right) \quad (6)$$

This step leads to a partially reconstructed snow cover map which is further enhanced in the next steps.

## 4.2 Monthly probability fields

Snow cover extent is a seasonally variable parameter. The probability of a certain pixel to be covered by snow or land varies with time. The second step for reconstructing snow cover is based on the idea that certain pixels within the basin are snow covered or snow free with high confidence during different months. This allows detecting temporally persistent (continuous snow/snow free coverage) spatial patterns of snow or

land cover for a certain month. Such spatial patterns can be identified using the available MODIS daily snow cover data in the period 2000–2012 and computing “monthly probability” (MP) of each pixel to be covered as snow or land in a certain month:

$$MP_{(x,y),(m)}^S = \frac{\sum (S_{(x,y,t),(t \in m)} = 1)}{N_{(x,y),(m)}} \quad (7)$$

$$MP_{(x,y),(m)}^L = \frac{\sum (S_{(x,y,t),(t \in m)} = 0)}{N_{(x,y),(m)}} \quad (8)$$

where  $MP_{(x,y),(m)}^S$  and  $MP_{(x,y),(m)}^L$  are the monthly probabilities of pixel  $x, y$  in month  $m$  for snow and land, respectively.  $S_{(x,y,t)}$  indicates the coverage (snow or land) of pixel  $x, y$  on day  $t$  of month  $m$ .  $N_{(x,y),(m)}$  is the number of total MODIS observations of pixel  $x, y$  and month  $m$  in the period 2000–2012. The value of  $MP_{(x,y),(m)}^S$  ( $MP_{(x,y),(m)}^L$ ) can be at maximum 1, meaning that the pixel  $x, y$  was covered always by snow (land) in month  $m$  during the cloud-free days in the period 2000–2012. Computation of MPs for every pixel in the study area leads to MP maps for all 12 months as illustrated exemplarily in Fig. 5 for April with  $MP^S$  and  $MP^L$  equal 1.

15 Pixels with  $MP_{(x,y),(m)}^S = 1$  in Fig. 5, i.e. pixels that were always snow covered in April, add up to 12.7% of the whole area. This means that 12.7% of the study area can be classified as snow covered in April. Pixels with  $MP_{(x,y),(m)}^L = 1$  add up to 14.9%, i.e. 14.9% of the domain can be classified as snow free in April. To remain consistent with the terminology used in the first step, we call the sum of pixels with  $MP_{(x,y),(m)}^S = 1$  ( $MP_{(x,y),(m)}^L = 1$ ) monthly SPI (LPI) value for snow (land). Monthly SPI and LPI are defined in a similar way as in step 1 (Eqs. 3 and 4).

25 The main idea in this step is to transfer these temporally persistent monthly spatial snow/land patterns ( $SPI_m/LPI_m$ ) to the past to reconstruct historical snow cover. However, the validity of these temporally persistent spatial snow/land patterns over longer time in the past is not assured, due to e.g. potential warmer/cooler or wetter/drier climate conditions. In order to account for possible climatic variability, we introduce

## Snow cover reconstruction methodology

A. Gafurov et al.

Title Page

Abstract

Introduction

Conclusions

References

Tables

Figures



Back

Close

Full Screen / Esc

Printer-friendly Version

Interactive Discussion



a buffer as vertical elevation shift from month-specific minimum snow and maximum land lines. We define a month-specific minimum snow line ( $H_{\min,m}^S$ ) and a month-specific maximum land line ( $H_{\max,m}^l$ ) as:

$$H_{\min,m}^S = \min(H_{x,y}) \quad \forall \quad MP_{(x,y,m)}^S = 1 \quad (9)$$

$$H_{\max,m}^l = \max(H_{x,y}) \quad \forall \quad MP_{(x,y,m)}^l = 1 \quad (10)$$

where  $H_{(x,y)}$  is the elevation of the pixel  $x, y$ .  $H_{\max,m}^l$  is thus the maximum elevation of all pixels with  $MP_{(x,y,m)}^l = 1$  in month  $m$ . Note that below the altitude  $H_{\max,m}^l$  not all pixels necessarily have  $MP_{(x,y,m)}^l = 1$ . Similarly,  $H_{\min,m}^S$  is the minimum elevation of all pixels with  $MP_{(x,y,m)}^S = 1$  in month  $m$ . Again,  $H_{\min,m}^S$  does not necessarily represent the elevation above which all pixels have  $MR_{(x,y,n)}^S = 1$ . Table 2 lists monthly SPI and LPI values, as well as  $H_{\min,m}^S$  and  $H_{\max,m}^l$  values for the selected area.

These  $H_{\min,m}^S$ ,  $H_{\max,m}^l$ , and monthly SPI/LPI maps were used to further reconstruct the snow cover resulting from step 1:

$$S_{(x,y)} = 1 \quad \text{if} \quad \left( H_{(y,x)} > H_{\min,m}^S + \text{buffer} \quad \text{and} \quad MR_{(x,y,m)}^S = 1 \right) \quad (11)$$

$$S_{(x,y)} = 0 \quad \text{if} \quad \left( H_{(y,x)} < H_{\max,m}^l - \text{buffer} \quad \text{and} \quad MR_{(x,y,m)}^l = 1 \right) \quad (12)$$

where buffer is a parameter accounting for the possible vertical shift in snow line. In order to account for climate variability not represented by the period for which satellite observations are available, “buffer” was set to 500 m. Due to absence of historical data on snow line variations in the region, the buffer was estimated corresponding to the maximum observed variation in the Equilibrium Line Altitude (ELA) of Abramov Glacier (Table 3, see Fig. 1 for location) for the period 1972–1998 (WGMS 2001; Pertziger 1996), and is, thus, a conservative estimate for the variations in snow line for the study area.

**Snow cover reconstruction methodology**

A. Gafurov et al.

Title Page

Abstract

Introduction

Conclusions

References

Tables

Figures



Back

Close

Full Screen / Esc

Printer-friendly Version

Interactive Discussion



### 4.3 Pixel to pixel matching-ratio fields

In step 1, MRs between each pixel and station were computed, and any pixel that had MR = 1 was classified according to the station record. The idea behind the third step is similar, but MRs between different pixels are computed this time. In such a way, the state of different pixels is used as a predictor for snow cover elsewhere. We define the MR between two pixels with coordinates  $x, y$  and  $i, j$  as:

$$MR_{(i,j),(x,y)}^s = \frac{\sum (1 - \text{ABS}(S_{i,j,t} - S_{x,y,t}))}{N_{(i,j)}} \quad \forall S_{x,y,t} = 1 \quad (13)$$

$$MR_{(i,j),(x,y)}^l = \frac{\sum (1 - \text{ABS}(S_{i,j,t} - S_{x,y,t}))}{N_{(i,j)}} \quad \forall S_{x,y,t} = 0 \quad (14)$$

where  $S_{i,j,t}$  indicates whether the pixel with coordinates  $i, j$  is snow covered ( $S = 1$ ) or snow free ( $S = 0$ ) for a given day  $t$ , and  $N_{(i,j)}$  is the total number of valid observations (clear sky, no cloud) at pixel  $i, j$  simultaneously available for a given condition ( $S_{x,y,t} = 1$  or  $S_{x,y,t} = 0$ ) in the period 2000–2012.

The computation of  $MR_{(i,j),(x,y)}^s$  and  $MR_{(i,j),(x,y)}^l$  according to Eqs. (13) and (14) is repeated in an “all-vs.-all” procedure, which means that all possible combinations of  $(x, y)$  and  $(i, j)$  are considered. For the region of interest, this yields at maximum 339552 ( $2 \times$  total number of pixels) MR maps (i.e. two maps for every pixel: for snow and land condition). However, not all of those maps were used for snow reconstruction since some pixels may have no dependence (no pixels with MR = 1) to any other pixel in the study area and were thus discarded. An example of the MR maps for snow and snow free conditions for the pixel located at  $x = 100$  and  $y = 100$  is given in Fig. 6.

The pixel with coordinates  $x = 100, y = 100$  has  $MR_{(i,j),(100,100)}^s = 1$  with 30684 (18%) other pixels in the study area, which means that when the particular pixel was snow covered during 2000–2012, 30684 other pixels were always snow covered as well. Thus, 18% is the SPI value of that pixel and can be interpreted as predictive

power for snow of the pixel for the entire study area. Analogously, 23 770 pixels (14 %) have  $MR_{(i,j),(100,100)}^l = 1$  with this pixel and is LPI value of this pixel. The SPI and LPI values of each pixel are derived through Eqs. (3) and (4) and illustrated in Fig. 7 for all pixels in the study area.

The maximum value of Fig. 7 (top) is 46 %, meaning that, according to the observations of the period 2000–2012, 46 % (78 189 pixels) of the study area was always snow covered when that particular pixel was snow covered. The maximum LPI value (Fig. 7 bottom) is 88 %, meaning that this particular pixel is able to predict snow free conditions for 88 % (149 685 pixels) of the basin. These two pixels with maximum SPI and LPI values are located within an area which has the highest predictive power for snow and land, respectively. When interpreting Fig. 7, three further features are worth notice: (1) pixels with SPI = 0 or LPI = 0 exist as well; these pixels have no predictive power and are therefore not used in the snow cover reconstruction; (2) SPI and LPI maps generally reflect the topography of the catchment: lower elevation pixels have higher SPI values and pixels at higher elevations have higher LPI values; (3) snow free pixels are easier to predict than snow covered ones.

The SPI and LPI maps were used for classifying pixels that are still undefined after the previous steps:

$$S_{(i,j,t)} = 1 \quad \text{if} \quad \left( MR_{(i,j),(x,y)}^s = 1 \quad \text{and} \quad S_{(x,y,t)} = 1 \right) \quad (15)$$

$$S_{(i,j,t)} = 0 \quad \text{if} \quad \left( MR_{(i,j),(x,y)}^l = 1 \quad \text{and} \quad S_{(x,y,t)} = 0 \right) \quad (16)$$

Since in this step SPI and LPI maps were generated for every pixel in the basin, this step tends to classify a significantly larger area than the first step where only 7 stations were used for constructing MRs.

**Snow cover reconstruction methodology**

A. Gafurov et al.

Title Page

Abstract

Introduction

Conclusions

References

Tables

Figures



Back

Close

Full Screen / Esc

Printer-friendly Version

Interactive Discussion



#### 4.4 Snow cover estimation using elevation information from neighbouring pixels

This step is adapted from Gafurov et al. (2009) and is based on the information of neighbouring pixels. Let us consider a pixel that has not been classified as snow covered or snow free in any of the previous steps. If any of the adjacent eight pixels is covered by snow and the elevation of that snow-covered pixel is lower than the pixel that is still undefined, then the undefined pixel is classified as snow covered. The same idea is applied for snow-free pixels. Hence, this step can be formalized as follows:

$$S_{(x,y,t)} = 1 \quad \text{if} \quad S_{(x+k,y+k,t)} = 1 \quad \text{and} \quad H_{(x+k,y+k)} < H_{(x,y)} \quad k \in (-1, 1) \quad (17)$$

$$S_{(x,y,t)} = 0 \quad \text{if} \quad S_{(x+k,y+k,t)} = 0 \quad \text{and} \quad H_{(x+k,y+k)} > H_{(x,y)} \quad k \in (-1, 1) \quad (18)$$

#### 4.5 Snow cover estimation with $MR < 1$

In the last step, the  $MR_{(x,y),(n)}^s$  and  $MR_{(x,y),(n)}^l$  values calculated in step 1 were used again. Whereas in step 1 only relations with  $MR = 1$  were considered, this step considers  $MR < 1$  relations to classify still undefined pixels. As illustrated in Fig. 4, MR values vary from 0 to 1. Such cases were considered in this step: still undefined pixels were classified according to the maximum MR value at this pixel (which however is  $< 1$ ) among 14 MR values (7 MRs for snow and 7 MRs for land) through Eqs. (19) and (20).

$$S_{(x,y,t)} = 1 \quad \text{if} \quad \max \left( MR_{(x,y,n)}^s \quad \forall S_{n,t} = 1 \right) > \max \left( MR_{(x,y,n)}^l \quad \forall S_{n,t} = 0 \right) \quad (19)$$

$$S_{(x,y,t)} = 0 \quad \text{if} \quad \max \left( MR_{(x,y,n)}^l \quad \forall S_{n,t} = 0 \right) > \max \left( MR_{(x,y,n)}^s \quad \forall S_{n,t} = 1 \right) \quad (20)$$

Taking maximum MR values for still undefined pixels in the last step allows to complete the classification for all pixels. However, since in this step  $MR < 1$  was considered, the reconstruction is subject to uncertainty that stems from non-perfect agreement between station records and a pixel in the period 2000–2012.

## 5 Results and discussion

Applying the five steps described above, snow cover maps for the area containing Zer-  
afshan basin were reconstructed for four days in 1998 and 1999. The maps contain  
binary information showing whether a given pixel was covered by snow or not. The  
accuracy of the reconstructed snow cover maps was assessed by comparing against  
independent snow maps derived from four Landsat images from the same days. The  
validation could be done only for recent years (1998 and 1999) due to availability of  
cloud free Landsat images during the snow period only for those days. The comparison  
was performed on a pixel-to-pixel basis, and the accuracy was assessed in a contin-  
gency table (Table 4). In Table 4, the sum of percentages of “SS” and “LL” columns  
represent the degree of accuracy after each reconstruction step, related to the total  
share of reconstructed pixels. Accordingly, the sum of “SL” and “LS” indicate the error  
in relation to the total percentage.

As an example, Fig. 8 shows the reconstructed and Landsat-derived snow cover  
maps for 10 April 1998. The comparison of these maps results in 86.4% of cor-  
rect reconstruction (cases SS + LL in Table 4) and 13.6% of erroneous reconstruction  
(SL + LS). Steps 1–4 show high accuracy with only little erroneous reconstruction (ER)  
whereas step 5 has the lowest accuracy in all validation days. However, the reconstruc-  
tion fraction (RF) is very high in step 5 compared to previous steps. Note that ER may  
also be enhanced by erroneous snow cover estimation from raw Landsat data and due  
to the spatial aggregation of Landsat 30 m original resolution to 500 m.

In order to better illustrate snow reconstruction in step 5, Fig. 9 shows the areal  
fraction for which the reconstruction was performed in steps 1–4 and maximum MRs  
obtained in step 5 under  $MR < 1$  condition for the validation day of April, 10. Most of the  
still unclassified pixels after steps 1–4 have MR values close to 1 and only few pixels  
have a lower MR value (reddish and light blue colours in Fig. 9). Figure 10 illustrates  
the trade-off between RF and ER as a function of MR in step 5. For example, for the  
validation day of 10 April, ER from steps 1–4 adds up to 1.5% (Table 4) and RF to

### Snow cover reconstruction methodology

A. Gafurov et al.

Title Page

Abstract

Introduction

Conclusions

References

Tables

Figures



Back

Close

Full Screen / Esc

Printer-friendly Version

Interactive Discussion



51.4% (snow and land classes in Fig. 9). With decreasing MR, RF increases, but at the cost of an increased ER. However, Fig. 10 also shows that RF is relatively high until about  $MR = 0.9$  with increasing ER. In all four days used for validation, an almost complete reconstruction is achieved with  $MR > 0.9$ .

Figures 8–10 also demonstrate that the methodology provides two types of results for snow cover reconstruction: deterministic and probabilistic snow cover maps. Deterministic maps result from the complete classification of pixels (Fig. 8) with binary information (snow/snow free) taking  $MR < 1$  in step 5 into account at the expense of the overall accuracy. However, the accuracy is still quite high with a range of 83.6–86.4% for the four validation days and is only slightly less than the accuracy of MODIS snow cover product in Central Asia (ca. 92%) when compared to Landsat snow information (Gafurov et al., 2013). Alternatively, probabilistic snow cover maps (Fig. 9) deliver a partial snow cover reconstruction with high accuracy resulting from steps 1–4, and, as result from step 5, a probability statement for snow cover for the remaining pixels.

## 6 Limitations of the methodology

The predictive power of the observations at meteorological stations for snow cover reconstruction is limited by the elevation range of the stations. If all meteorological stations are located at high elevations, they will be good predictors during summer for snow-free conditions, but will perform poorly when predicting snow-covered areas during winter due to their elevation and correspondingly lower SPI values. Conversely, low-elevation stations are better indicators for snow-covered pixels at higher altitudes than they are for snow-free ones. Hence, a wide spread in station elevation is optimal for accurate snow cover reconstruction. In our case study, the application of the presented methodology suffered from the small number of station data (only 7 stations). A higher number of stations would lead to a higher number of SPI and LPI maps and

### Snow cover reconstruction methodology

A. Gafurov et al.

Title Page

Abstract

Introduction

Conclusions

References

Tables

Figures



Back

Close

Full Screen / Esc

Printer-friendly Version

Interactive Discussion



would allow to reconstruct a larger areal fraction of snow cover in the first four steps. Noticeably, the stations do not need to be located inside the area of interest.

Reconstruction of the snow cover for the past is based on the assumptions that (1) the calibration period, i.e. the MODIS data period, is representative for the past period, and (2) the relationship between station records and spatial snow patterns derived from MODIS data is stationary, i.e. does not significantly change in time. A calibration period which lacks extreme conditions, e.g. snow-rich or snow-scarce years, might lead to larger errors in the reconstruction. A longer calibration period is expected to lead to more robust relationships for reconstructing snow cover.

The problem of representativity of the MODIS period in the reconstruction step 2 is tackled by the introduction of the elevation buffer to capture the effect of inter-annual temporal variability of snow line elevation. For this the temporal variability of the recorded ELA from the neighbouring Abramov glacier was used as a proxy. Through changes in climatic conditions of the calibration period going beyond temporal variability of the snow line elevation in the reconstruction period, the relationships between station records and some pixels (step 1) and between pixels (step 3) may become non-representative. This occurs if snow line in the future/calibration period more often separates the station of the pixels compared to the reconstruction period. Hence, an analysis of temperature and precipitation trends and comparison of climatology between calibration and reconstruction periods may provide some confidence on representativeness of the relationships used.

## 7 Conclusions

In this study, a methodology for reconstructing past snow cover using historical in situ snow depth data, recent remote sensing snow cover data and topographic data was presented. The methodology is based on (1) constructing relationships between station observations and remote sensing data, (2) estimating the monthly variation of snow cover from remote sensing data, (3) deriving pixel-to-pixel relationships using remote

### Snow cover reconstruction methodology

A. Gafurov et al.

Title Page

Abstract

Introduction

Conclusions

References

Tables

Figures



Back

Close

Full Screen / Esc

Printer-friendly Version

Interactive Discussion



sensing data, and (4) using neighbourhood relations. Once the dependence between individual pixels and station records is derived, this dependence is used to reconstruct past snow cover based solely on station records.

The methodology was applied to a study area containing the Zerafshan River basin – a basin with high topographic gradients – in Central Asia and showed correct classification in the range of 83.6 to 86.4 % when compared to four Landsat snow cover scenes. This high agreement is noteworthy, given that only 7 stations and 12 years of remote sensing data were available. The agreement is only slightly less than of original MODIS snow cover product with accuracy of about 92 % for Central Asia when compared to Landsat (Gafurov et al., 2013). Just 12 years of MODIS data were sufficient to extract stable patterns of snow cover and relate them to station records. Hence, we conclude that the developed methodology is suitable to derive past snow cover in remote mountainous regions with very limited data availability. Reconstructed snow cover patterns can be used for hydrological model calibration/validation and for understanding snow cover dynamics over large areas prior the age of satellite observations.

*Acknowledgement.* This work was carried out in the frame of the CAWa (Water in Central Asia) project (<http://www.cawa-project.net>, Contract No. AA7090002), funded by the German Federal Foreign Office as part of the “Berlin Process”. Doris Duethmann was supported by the SuMaRiO project (Sustainable Management of River Oases along the Tarim River/China), funded by the BMBF (German Ministry for Education and Research) – Funding Measure “Sustainable Land Management”, reference number: LLA2-02.

## References

- Aizen, V., Aizen, E., and Melack, J.: Climate snow cover, glaciers and runoff in the Tien Shan, Central Asia, *Water Resour. Bull.*, 31, 1113–1129, 1995.
- Ault, T., Czajkowski, K., Benko, T., Coss, J., Struble, J., Spongberg, A., Templin, M., and Gross, C.: Validation of the MODIS snow product and cloud mask using student and NWS cooperative station observations in the Lower Great Lakes Region, *Remote Sens. Environ.*, 105, 341–353, 2006.

## Snow cover reconstruction methodology

A. Gafurov et al.

Title Page

Abstract

Introduction

Conclusions

References

Tables

Figures



Back

Close

Full Screen / Esc

Printer-friendly Version

Interactive Discussion



## Snow cover reconstruction methodology

A. Gafurov et al.

Title Page

Abstract

Introduction

Conclusions

References

Tables

Figures



Back

Close

Full Screen / Esc

Printer-friendly Version

Interactive Discussion



- Brown, E.: Northern Hemisphere snow cover variability and change, 1915–97, *J. Climate*, 13, 2339–2355, 1999.
- Corbari, C., Ravazzani, G., Martinelli, J., and Mancini, M.: Elevation based correction of snow coverage retrieved from satellite images to improve model calibration, *Hydrol. Earth Syst. Sci.*, 13, 639–649, doi:10.5194/hess-13-639-2009, 2009.
- Duethmann, D., Peters, J., Blume, T., Vorogushyn, S., and Güntner, A.: The value of satellite-derived snow cover images for calibrating a hydrological model in snow-dominated catchments in Central Asia, *Water Resour. Res.*, 50, 2002–2021, doi:10.1002/2013WR014382, 2014.
- Durand, M., Molotch, N., and Margulis, A.: A Bayesian approach to snow water equivalent reconstruction, *J. Geophys. Res.*, 113, D20117, doi:10.1029/2008JD009894, 2008.
- Erickson, T., Williams, M., and Winstral, A.: Persistence of topographic controls on the spatial distribution of snow in rugged mountain terrain, Colorado, United States, *Water Resour. Res.*, 41, W04014, doi:10.1029/2003WR002973, 2005.
- Finger, D., Pellicciotti, F., Konz, M., Rimkus, S., and Burlando, P.: The value of glacier mass balance, satellite snow cover images and hourly discharge for improving the performance of a physically based distributed hydrological model, *Water Resour. Res.*, 47, W07519, doi:10.1029/2010WR009824, 2011.
- Frei, A., Robinson, D., and Hughes, M.: North American snow extent: 1900–1994, *Int. J. Climatol.*, 19, 1517–1534, 1999.
- Gafurov, A. and Bárdossy, A.: Cloud removal methodology from MODIS snow cover product, *Hydrol. Earth Syst. Sci.*, 13, 1361–1373, doi:10.5194/hess-13-1361-2009, 2009.
- Gafurov, A., Kriegel, D., Vorogushyn, S., and Merz, B.: Evaluation of remotely sensed snow cover product in Central Asia, *Hydrol. Res.*, 44, 506–522, doi:10.2166/nh.2012.094, 2013.
- Hall, D., Riggs, G., and Salomonson, V.: Development of methods for mapping global snow cover using Moderate Resolution Imaging Spectroradiometer (MODIS) data, *Remote Sens. Environ.*, 83, 181–194, 2002.
- Hall, D., Riggs, G., Foster, J., and Kumar, S.: Development and evaluation of a cloud-gap-filled MODIS daily snow-cover product, *Remote Sens. Environ.*, 114, 496–503, 2010.
- Huang, X., Liang, T., Zhang, X., and Guo, Z.: Validation of MODIS snow cover products using Landsat and ground measurements during the 2001–2005 snow seasons over northern Xinjiang, China, *Int. J. Remote Sens.*, 32, 133–52, 2011.

## Snow cover reconstruction methodology

A. Gafurov et al.

Title Page

Abstract

Introduction

Conclusions

References

Tables

Figures



Back

Close

Full Screen / Esc

Printer-friendly Version

Interactive Discussion



Immerzeel, W., Droogers, P., Jong, S., and Bierkens, M.: Large-scale monitoring of snow cover and runoff simulation in Himalayan river basins using remote sensing, *Remote Sens. Environ.*, 113, 40–49, 2008.

Jarvis, A., Reuter, H., Nelson, A., and Guevara, E.: Hole-filled SRTM for the globe Version 4, available from the CGIAR-CSI SRTM 90 m Database, <http://srtm.csi.cgiar.org> (last access: 30 March 2008), 2008.

Klein, A., Barnett, A., and Lee, S.: Evaluation of MODIS snow cover products in the upper Rio Grande River Basin, EGS – AGU – EUG Joint Assembly, Nice, France, 6–11 April 2003, abstract number: 12420, 2003.

Liang, T., Zhang, X., Xie, H., Wu, C., Feng, Q., Huang, X., and Chen, Q.: Toward improved daily snow cover mapping with advanced combination of MODIS and AMSR-E measurements, *Remote Sens. Environ.*, 112, 3750–3761, 2008.

Li, X. and Williams, M.: Snowmelt runoff modeling in an arid mountain watershed, Tarim Basin, China, *Hydrol. Process.*, 22, 3931–3940, 2008.

Liu, T., Willems, P., Feng, X., Li, Q., Huang, Y., Bao, A., Chen, X., Veroustraete, F., and Dong, Q.: On the usefulness of remote sensing input data for spatially distributed hydrological modeling: case study of the Tarim River basin in China, *Hydrol. Process.*, 26, 335–344, 2012.

López-Burgos, V., Gupta, H. V., and Clark, M.: Reducing cloud obscuration of MODIS snow cover area products by combining spatio-temporal techniques with a probability of snow approach, *Hydrol. Earth Syst. Sci.*, 17, 1809–1823, doi:10.5194/hess-17-1809-2013, 2013.

NASA Landsat Program, Landsat TM and ETM+, USGS, Sioux Falls, 2003.

Ososkova, T., Gorelkin, N., and Chub, V.: Water resources of Central Asia and adaptation measures for climate change, *Environ. Monit. Assess.*, 61, 161–166, 2000.

Parajka, J. and Blöschl, G.: Validation of MODIS snow cover images over Austria, *Hydrol. Earth Syst. Sci.*, 10, 679–689, doi:10.5194/hess-10-679-2006, 2006.

Parajka, J. and Blöschl, G.: The value of MODIS snow cover data in validating and calibrating conceptual hydrological models, *J. Hydrol.*, 358, 240–258, 2008a.

Parajka, J. and Blöschl, G.: Spatio-temporal combination of MODIS images – potential for snow cover mapping, *Water Resour. Res.*, 44, 1–13, 2008b.

Parajka, J., Holko, L., Kostka, Z., and Blöschl, G.: MODIS snow cover mapping accuracy in a small mountain catchment – comparison between open and forest sites, *Hydrol. Earth Syst. Sci.*, 16, 2365–2377, doi:10.5194/hess-16-2365-2012, 2012.

## Snow cover reconstruction methodology

A. Gafurov et al.

Title Page

Abstract

Introduction

Conclusions

References

Tables

Figures



Back

Close

Full Screen / Esc

Printer-friendly Version

Interactive Discussion



Pellicciotti, F., Buegri, C., Immerzeel, W., Konz, M., and Shrestha, A.: Challenges and uncertainties in hydrological modeling of remote Hindu-Kush-Karakoram-Himalayan (HKH) Basins: suggestions for calibration strategies, *Mt. Res. Dev.*, 39, 39–50, 2012.

Pertziger, F.: *Abramov Glacier Data Reference Book: Climate, Runoff, Mass Balance*, Technical University Munich, Tashkent/Munich, 1996.

Robinson, D.: Merging operational satellite and historical station snow cover data to monitor climate change, *Palaeogeogr. Palaeoclimatol.*, 90, 235–240, 1991.

Tekeli, A., Akyurek, Z., Sorman, A., Sensoy, A., and Sorman, A.: Using MODIS snow cover maps in modeling snowmelt runoff process in the eastern part of Turkey, *Remote Sens. Environ.*, 97, 216–230, 2005.

Tong, J., Déry, S. J., and Jackson, P. L.: Interrelationships between MODIS/Terra remotely sensed snow cover and the hydrometeorology of the Quesnel River Basin, British Columbia, Canada, *Hydrol. Earth Syst. Sci.*, 13, 1439–1452, doi:10.5194/hess-13-1439-2009, 2009.

Unger-Shayesteh, K., Vorogushyn, S., Farinotti, D., Gafurov, A., Duethmann, D., Mandychew, A., and Merz, B.: What do we know about past changes in the water cycle of Central Asian headwaters? A review, *Global Planet. Change*, 110, 4–25, doi:10.1016/j.gloplacha.2013.02.004, 2013.

Wang, X., Xie, H., and Liang, T.: Evaluation of MODIS snow cover and cloud mask and its application in Northern Xinjiang, China, *Remote Sens. Environ.*, 112, 1497–1513, 2008.

Wang, J., Li, H., and Hao, X.: Responses of snowmelt runoff to climatic change in an inland river basin, Northwestern China, over the past 50 years, *Hydrol. Earth Syst. Sci.*, 14, 1979–1987, doi:10.5194/hess-14-1979-2010, 2010.

WGMS: *Glacier Mass Balance Bulletin No. 6 (1998–1999)*, edited by: Haeberli, W., Frauenfelder, R., and Hoelzle, M., IAHS (ICSU)/UNEP/UNESCO, World Glacier Monitoring Service, Zurich, available at: [http://www.wgms.ch/mbb/mbb6/wgms\\_2001\\_gmbb6.pdf](http://www.wgms.ch/mbb/mbb6/wgms_2001_gmbb6.pdf) (last access: 4 January 2013), 2001.

Zhou, H., Aizen, E., and Aizen, V.: Deriving long term snow cover extent dataset from AVHRR and MODIS data: Central Asia case study, *Remote Sens. Environ.*, 136, 146–162, doi:10.1016/j.rse.2013.04.015, 2013.







## Snow cover reconstruction methodology

A. Gafurov et al.

Title Page

Abstract

Introduction

Conclusions

References

Tables

Figures

◀

▶

◀

▶

Back

Close

Full Screen / Esc

Printer-friendly Version

Interactive Discussion



**Table 4.** Contingency table (in %) for the reconstructed snow cover maps validated against four aggregated Landsat snow cover images. Four cases are distinguished: SS, LL, SL, and LS. The first (second) letter indicates the classification according to the presented algorithm (Landsat). “S” stands for “snow”, “L” for “land”. “Total” indicates the percentage of pixels classified after each step. Results refer to the Landsat domain (dashed line) shown in Fig. 1b.

Day	Step	SS	LL	SL	LS	Total
10 Apr 1998	1	8.5	7.2	0.0	0.0	15.7
	2	13.0	14.9	0.1	0.1	28.1
	3	17.5	27.1	0.8	0.1	45.5
	4	20.6	29.3	1.3	0.2	51.4
	5	44.3	42.1	11.6	2.0	100.0
20 Nov 1998	1	0.1	11.2	0.0	0.0	11.3
	2	0.2	11.3	0.0	0.0	11.5
	3	0.5	30.5	0.0	0.0	31.0
	4	1.4	33.4	0.0	0.1	34.9
	5	18.2	66.6	2.1	13.1	100.0
29 Apr 1999	1	0.1	13.9	0.0	0.0	14.0
	2	7.6	21.5	0.0	0.5	29.6
	3	9.0	35.2	0.1	0.7	45.0
	4	11.0	38.1	0.3	0.9	50.3
	5	24.9	58.7	13.9	2.5	100.0
15 Nov 1999	1	18.4	4.1	0.0	0.4	22.9
	2	18.4	4.2	0.0	0.4	23.0
	3	24.8	15.7	0.4	0.8	41.7
	4	28.5	18.3	0.7	1.3	48.9
	5	42.3	41.7	10.6	5.4	100.0

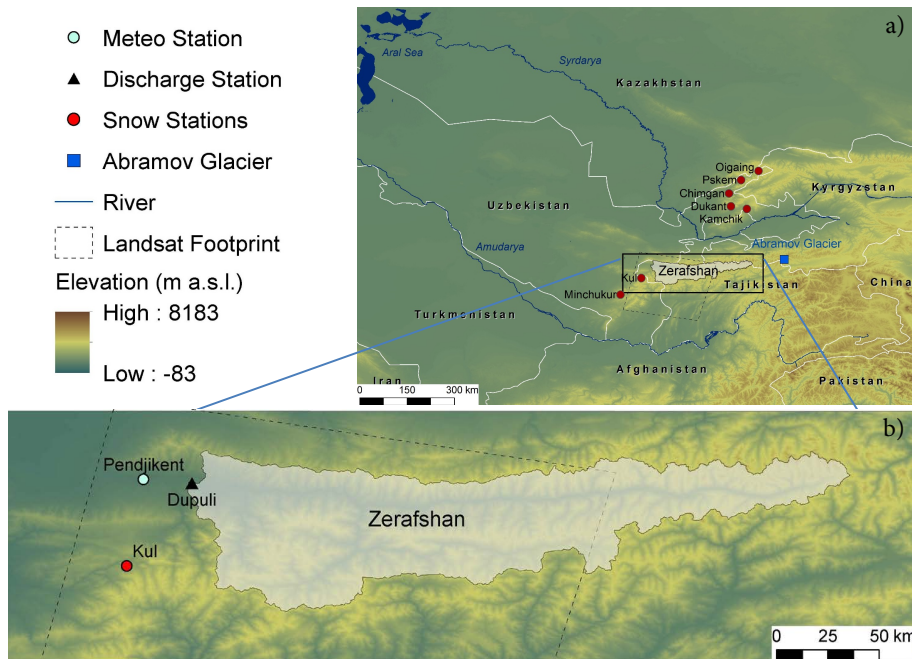


**Figure 1.** Location of the Upper Zerafshan River basin in the Gissaro-Alai Mountain Range, Central Asia. Snow cover reconstruction was conducted for the entire area of **(b)** and validated for the area with Landsat footprint.

**Snow cover reconstruction methodology**

A. Gafurov et al.

Title Page	
Abstract	Introduction
Conclusions	References
Tables	Figures
◀	▶
◀	▶
Back	Close
Full Screen / Esc	
Printer-friendly Version	
Interactive Discussion	





## Snow cover reconstruction methodology

A. Gafurov et al.

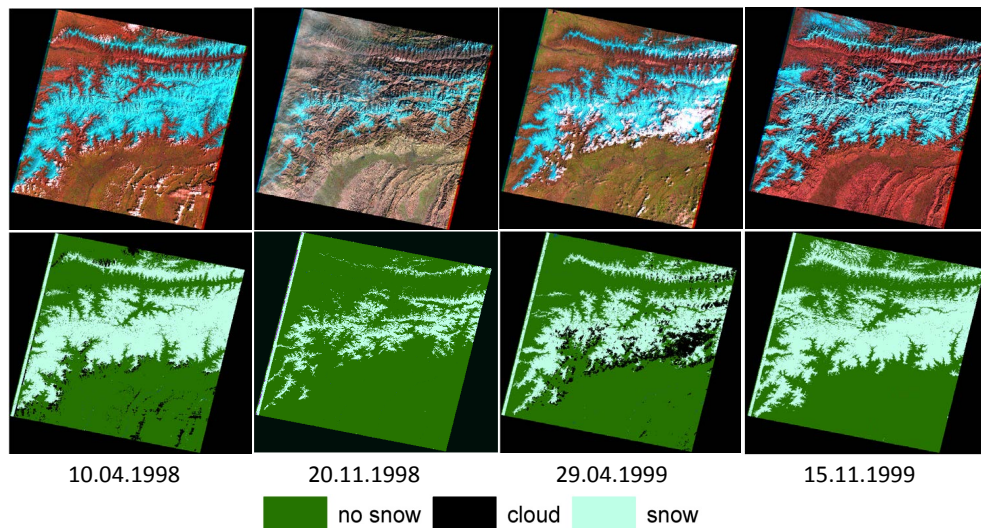


**Figure 3.** Original Landsat scenes (top row) and derived snow cover maps used for validation (bottom row). See Fig. 1a for areal coverage of Landsat footprint.

[Title Page](#)[Abstract](#)[Introduction](#)[Conclusions](#)[References](#)[Tables](#)[Figures](#)[◀](#)[▶](#)[◀](#)[▶](#)[Back](#)[Close](#)[Full Screen / Esc](#)[Printer-friendly Version](#)[Interactive Discussion](#)





## Snow cover reconstruction methodology

A. Gafurov et al.

Title Page

Abstract

Introduction

Conclusions

References

Tables

Figures

◀

▶

◀

▶

Back

Close

Full Screen / Esc

Printer-friendly Version

Interactive Discussion

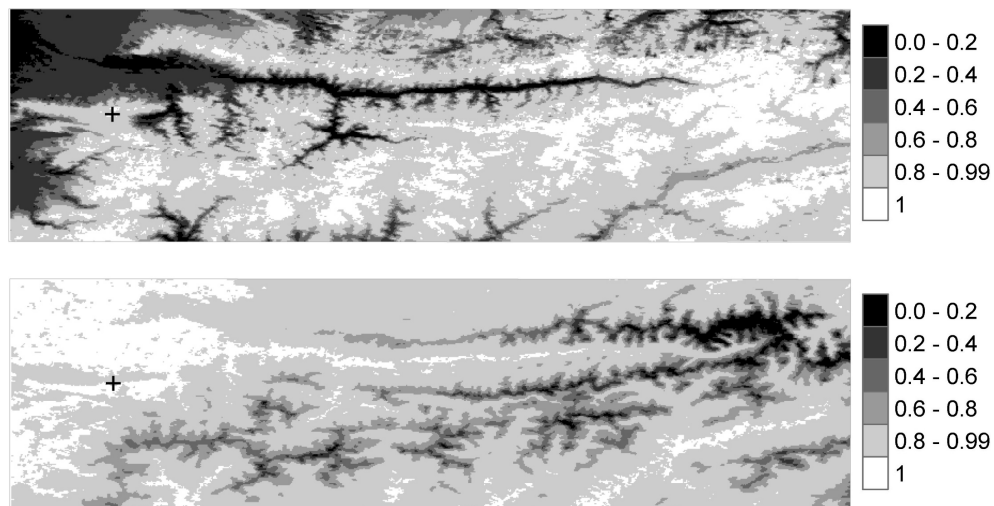


**Figure 6.**  $MR^s_{(i,j),(100,100)}$  (top) and  $MR^l_{(i,j),(100,100)}$  (bottom) fields for the pixel  $x = 100$ ,  $y = 100$  (black cross) with elevation 2206 m a.s.l.

## Snow cover reconstruction methodology

A. Gafurov et al.

Title Page

Abstract

Introduction

Conclusions

References

Tables

Figures



Back

Close

Full Screen / Esc

Printer-friendly Version

Interactive Discussion

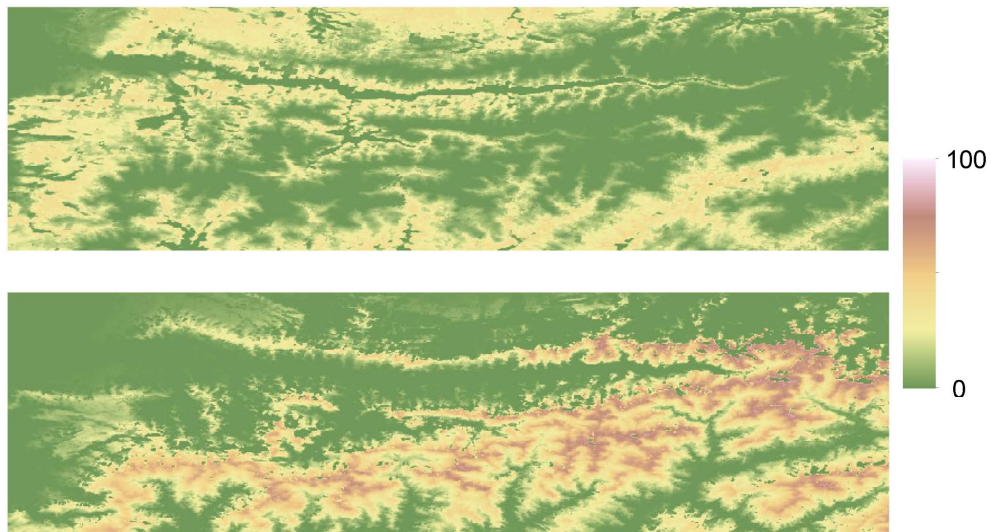


**Figure 7.** SPI (top) and LPI (bottom) values of each pixel (in %) in the study area defined in Fig. 1b.

## Snow cover reconstruction methodology

A. Gafurov et al.

Title Page

Abstract

Introduction

Conclusions

References

Tables

Figures

◀

▶

◀

▶

Back

Close

Full Screen / Esc

Printer-friendly Version

Interactive Discussion

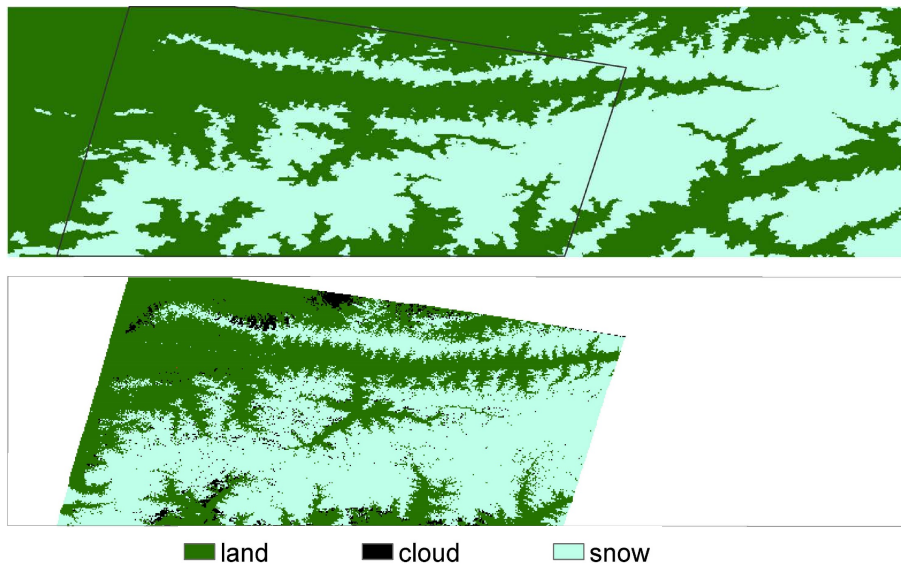


**Figure 8.** Reconstructed (top) and Landsat (bottom) snow cover maps for 10 April 1998.



